Defence Science Journal, Vol. 74, No. 2, March 2024, pp. 181-188, DOI : 10.14429/dsj.74.19667

Scramjet Intake Aerodynamic Studies Using Sharp-Interface Immersed Boundary Method

Amrita Pathak*, Jubajyoti Chutia and Vinayak Kulkarni

Department of Mechanical Engineering, Indian Institute of Technology Guwahati– 781 039, India
**E-mail: pathakamrita5@gmail.com*

ABSTRACT

In this present article, the use of a throttling device in the form of movable flap to study scramjet inlet unstart has been investigated numerically. The flap has been employed as an effort to simulate the rise in combustor pressure of the scramjet. Computational analysis for freestream Mach number and freestream pressure of 6.0 and 488 M respectively, have been performed by a two-dimensional compressible CFD in-house Finite volume solver for perfect gas. Convective fluxes have been evaluated using AUSM scheme. Inviscid flow has been assumed for all the simulations. Particular point of interest in these simulations is the application of Immersed Boundary Method along the wall boundaries, enabling the use of structured grid for complex geometries. The results demarcate the starting condition of the inlet based on the flap throttling values. Comparative results in the form of Mach number and pressure contours are presented for different flap positions. The use of Immersed Boundary Method has been successfully displayed by simulating a movable flap.

Keywords: Unstart; Scramjet; Immersed boundary method; Computational fluid dynamics

NOMENCLATURE

σ	: Radar cross section
K	: Boltzmann constant
B	: Boundary
∞	: Free stream conditions
d	: Domain
u	: x-direction velocity (m/s)
v	: y-direction velocity (m/s)
E	: Energy (J)
p	: Pressure (Pa)
ρ	: Density (kg/m^3)
τ	: Heat flux (N/m^2)
μ	: Coefficient of dynamic viscosity (Pa s)
M	: Mach number
T	: Temperature (K)
R	: Universal gas constant (J/K mol)
V_∞	: Freestream primitive variables
V_b	: Boundary primitive variables
V_d	: Domain primitive variables

1. INTRODUCTION

As the demand for high-speed propulsion continues to rise, significant endeavours are being made to develop efficient and safe air-breathing vehicles capable of operating at supersonic and hypersonic speeds. Among these vehicles, the scramjet engine stands out as a promising solution that can meet these desired expectations. Despite the initiation of research on hypersonic flight as early as the 1960s, substantial advancements and successful developments have predominantly occurred in recent decades. Notably, the HyperX/X-43A[1] project demonstrated remarkable achievements in terms of airframe integration and propulsion technology, thereby laying a solid foundation for the future development of hypersonic vehicles.

In the domain of hypersonic flight, scramjet engines have emerged as the most efficient propulsion system. Extensive experimental and numerical investigations have been conducted on scramjet engines, with particular emphasis placed on their aerodynamic performance. Among the unfavourable phenomena that can significantly impact the aerothermodynamic efficiency of scramjets, the occurrence of ‘unstart’ has gathered significant attention[2-8]. Unstart refers to a series of events in which an increase in downstream backpressure causes flow constriction, leading to an upstream propagation of a wave that disrupts the established configuration of oblique shock waves within the isolator. This disruption results in flow spillage from the inlet, leading to mass loss and, in extreme cases, engine stall. The occurrence of unstart can be attributed to one or a combination of factors, including flow choking, mass injection in the combustor, interactions between shock waves and boundary layers, and high inlet compression ratios.

Significant research efforts have been dedicated to investigating the phenomenon of unstart, employing both experimental techniques conducted in wind tunnels[4-8], as well as various numerical methodologies, including

Received : 29 November 2023, Revised : 11 January 2024
Accepted : 12 January 2024, Online published : 26 March 2024

Computational Fluid Dynamics (CFD)[3-10], and Reduced Order Models[11]. However, due to the unique and transient nature of the flow patterns observed during unstart in different inlet configurations, the process becomes highly intricate and demands further exploration.

To replicate the occurrence of flow choking observed in actual flight conditions, researchers often resort to the use of flow blockages as a means of generating downstream pressure rises under low-enthalpy conditions. This method has gained popularity due to its relative ease of implementation compared to incorporating a combustor within the inlet system. Alternative methods such as mass injection[13], movable cowl[15], or movable ramp have been employed in experimental setups to simulate the onset of unstart. In order to mimic unstart in wind tunnel or shock tunnel experiments, as well as in computational fluid dynamics (CFD)-based studies, researchers such as Wagner[5], et al. have utilized flaps to induce an increase in back pressure. Other studies conducted by Zhang[14], et al. and Tan[15], et al. have also presented investigations involving the use of mechanical blockages.

In this article, as a means of reducing the burden of experimental costs and to deal with the complexities of the flow, a numerical tool in the form of a sharp interface Immersed Boundary method (IBM)[16-17] has been accounted for scramjet applications. IBM is a numerical technique used for simulating fluid-structure interactions. It's widely used to analyse the movement of fluid around complex shapes. The fundamental concept of IBM is to consider the structure as an object submerged in the fluid instead of a rigid boundary, which enables more realistic and versatile simulations of the interactions between the fluid and the structure. In this article, the onset of unstart and corresponding flow dynamics are examined using an in-house Finite-volume solver in which the boundary conditions are enforced by utilizing Sharp-Interface IBM. The subsequent sections present a comprehensive discussion of the methodology used and the results obtained through this numerical formulation.

2. NUMERICAL METHODOLOGY

Provide sufficient detail to allow the work to be reproduced. Methods already published should be indicated by a reference: only relevant modifications should be described. Discuss Materials, Experimental setup and Instrumentation related to your research.

2.1 Governing Equations

For the present study, the Euler equations (mass, momentum and energy conservation) are solved using the finite volume method, which collectively can be expressed by Eqn. 1.

$$\frac{\partial U}{\partial t}+\frac{\partial F_I}{\partial x}+\frac{\partial G_I}{\partial y}=0 \tag{1}$$

where,

$$U=\begin{bmatrix}\rho\\ \rho u\\ \rho v\\ \rho E\end{bmatrix};F_I=\begin{bmatrix}\rho u\\ \rho u^2+p\\ \rho uv\\ \rho u\left(E+\frac{p}{\rho}\right)\end{bmatrix};G_I=\begin{bmatrix}\rho v\\ \rho uv\\ \rho v^2\\ \rho v\left(E+\frac{p}{\rho}\right)\end{bmatrix}$$

The equation of state is taken into account to obtain a closed-form system of equations, by assuming the fluid to behave like a perfect gas. It is given as,

$$P=\rho RT \tag{2}$$

The current numerical studies have been conducted by assuming the flow conditions to be inviscid.

2.2 Finite Volume Approach

The Eqn. 1 is rewritten in a discrete manner as,

$$\frac{d\vec{U}_i}{dt}=-\frac{1}{\Omega_i}\sum_{J\in i}H_{\perp_J}\Delta S_J=R(\vec{U}_i) \tag{3}$$

In Eqn. 3, summation is over all faces of the cell i and $H_\perp$ is the normal component of fluxes (F_I and G_I) to the respective face. $R(\vec{U}_i)$ is referred to as the residual term. The convective fluxes, F_I and G_I are evaluated using AUSM[18] scheme. Furthermore, a second order accurate reconstruction of flow properties along with Venkatkrishnan limiter[19] has been implemented to evaluate the flow properties at the cell faces as required by convective flux scheme. A low storage explicit Runge-Kutta (LSERK) scheme[19] is used to achieve second order temporal accuracy. The data structure of the flow solver is kept unstructured. The finite volume solver has been incorporated with a ghost cell Immersed Boundary Method which is elaborated in the following section.

2.3 Immersed Boundary Method

In the current problem, a movable flap is placed at the aft of the isolator which has to be deployed once the flow is stabilized for a flap-less flow condition. Thus, to solve this problem, we integrate the Immersed Boundary Method (IBM) in our solver. The details of the equations incorporated in our solver can be found in Ghias[16], *et al.* In this approach, fluid, solid and ghost cells are classified by their cell centres, where solid cells have their centres inside solid boundaries and fluid cells have their centres outside solid boundaries. ghost cells are the solid cells that lie in a finite volume stencil of a fluid cell. The different cell classifications are illustrated in Fig. 1 for representation purpose. The ghost cells' image points are determined by reflecting their centres across the solid boundary. The primitive variables at the image points are then calculated using bilinear interpolation. Finally, the ghost cell values are calculated by enforcing the boundary condition at the body's intersection along the line connecting the image point to the ghost cell centre. By the implementation of this IBM approach, the flap was superimposed as a solid boundary over an existing solution of the domain with the pre-existing background mesh and thus eliminated the complexities related with a moving mesh.

2.4 Solver Validation

In order to validate the in-house solver, a specific testcase is chosen from Ganesh & John[20], involving the simulation of hypersonic flow over a hemispherical model with a radius of 30 mm. The freestream conditions for the flow consist of a Mach number of 8, a static temperature of 113 K, and a static pressure of 89 Pa. For the purpose of this study, a moderately fine mesh comprising 68,338 grid cells has been employed.

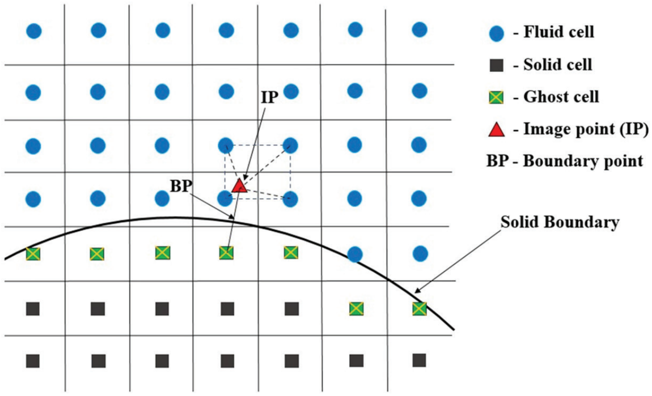

Figure 1. Illustration of the different cell types used in Immersed Boundary Method (IBM).

The computational domain, along with the grid details, are presented in Fig. 2(a). It can be observed that the grid is refined near the wall of the hemisphere, as displayed in the zoomed view. The yellow line depicts the surface of the body. This is achieved through the use of an adaptive grid resolution technique, details of which are provided in the following section.

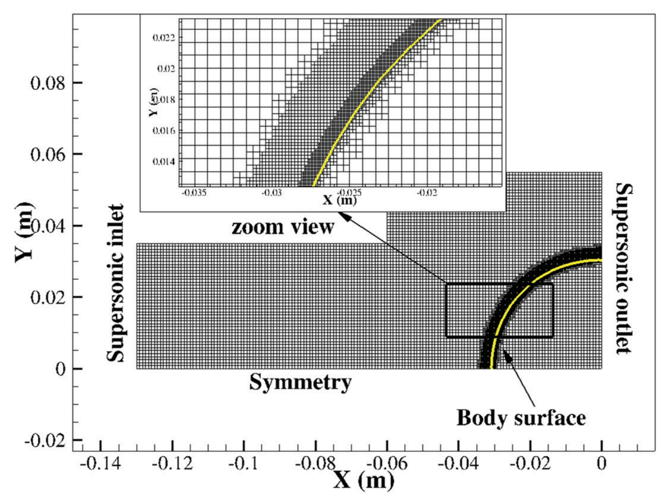

(a)

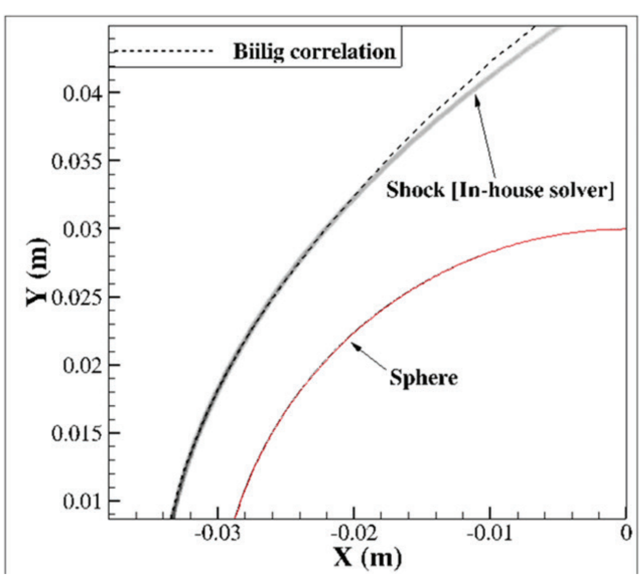

(b)

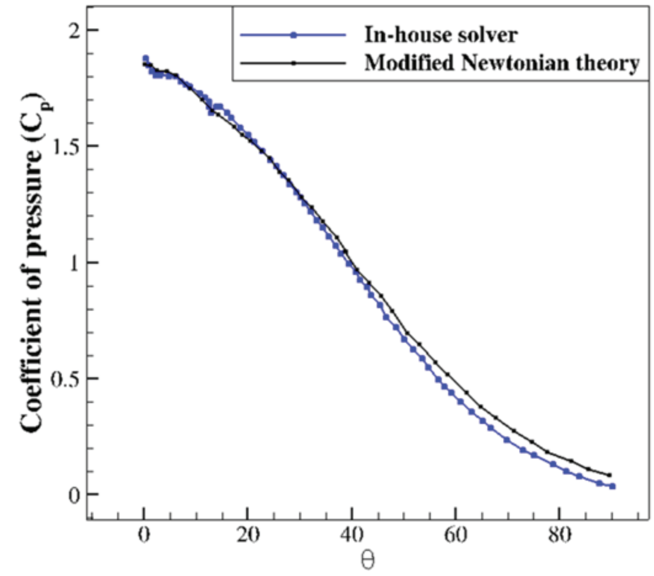

(c)

Figure 2. Grid and validation plots for hypersonic flow over hemisphere for Solver validation, (a) Computational domain with boundary conditions; (b) Shock shape comparison of Billig[21] with numerical solution obtained from in-house solver; and (c) Comparison of C_P *vs* θ for hemispherical body.

The accuracy of the solver is evaluated based on the shape of the shock, which is quantitatively assessed using the Billig[21] correlation (Eqn. 4), given as,

$$x = R + \delta - R_C \cot^2\beta\left[\left(1+\frac{y^2\tan^2\beta}{R_C}\right)^{\frac{1}{2}} - 1\right] \tag{4}$$

In Eqn. 4, R represents the nose radius of the sphere, while R_C denotes the radius of curvature of the shock wave centred on the vertex of the hyperbola. The expression for R_C is defined as follows:

$$\frac{R_C}{R} = 1.143\exp\left[\frac{0.54}{(M_\infty - 1)^{1.2}}\right] \tag{5}$$

Within Eqn. 5, the angle β represents the shock wave angle at an infinite distance from the stagnation point of the sphere. It is worth noting that approximating this angle as the Mach angle $\left(\phi = \sin^{-1}(1/M_\infty)\right)$ will not significantly impact the prediction of the shock shape in the case of hypersonic flow over the sphere. Figure 2(b) provides a comparison between the shock shape derived from the simulation and the empirical relation specified in Eqn. 4, demonstrating a high level of agreement between the two.

Additionally, a comparison is made between the surface pressure coefficient obtained from the simulation to that derived from the modified Newtonian theory[22]. The modified Newtonian theory provides a distribution of the pressure coefficient (C_p) over the surface of the sphere, which is expressed in Eqn. 6 as:

$$C_p = C_{pmax}\,\mathrm{Sin}^2\theta \tag{6}$$

where, (C_{pmax}) represents the maximum value of the pressure coefficient (C_p) at the stagnation point, while θ denotes the inclination of the local velocity vector on the surface of the sphere in relation to the freestream direction. By examining Fig. 2(c), it becomes apparent that the predictions made by the solver closely align with the predictions outlined by the modified Newtonian theory.

2.5 Computational Domain and Boundary Conditions

A mixed compression scramjet inlet model[23], as shown in Fig. 3(a), is employed for the current studies. It consists of two external ramps. From Fig. 3(a), it can be seen that a flap (F) is placed at the aft of the isolator, which will be deployed at different angles for different cases.

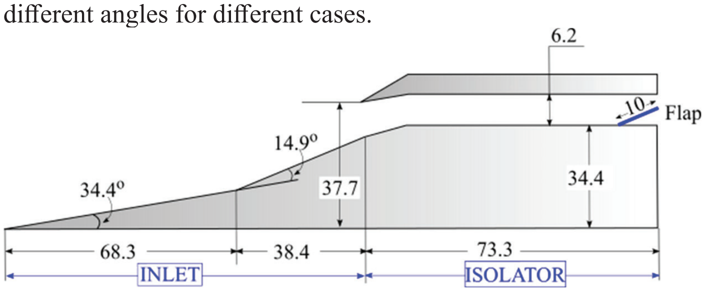

(a)

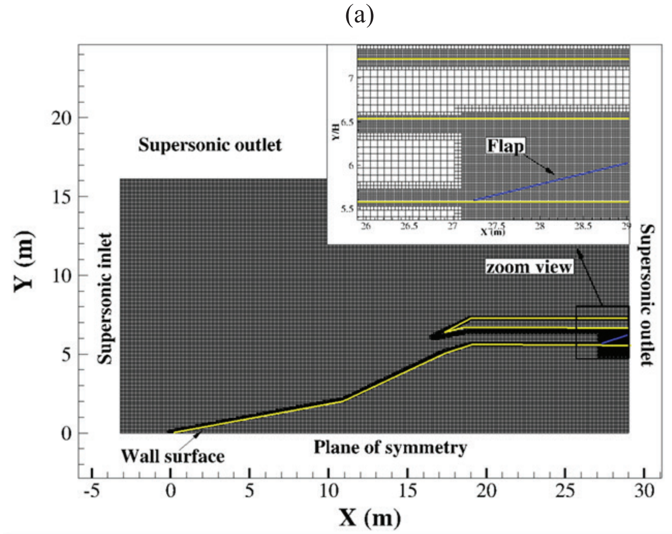

(b)

Figure 3. (a) Schematic diagram; and (b) grid domain along with the applied boundary conditions for the scramjet model.

The computational domain used for the present analysis is displayed in Fig. 3(b). The scramjet surface is marked by yellow lines and the flap near the isolator is marked by blue line. The inlet and outlet boundaries are considered as supersonic, as shown in Fig. 3(b). In supersonic inflow, boundary primitive variables are derived from the freestream variables $\left(\vec{V}_b = \vec{V}_\infty\right)$ and in supersonic outlet, primitive variables at the boundary are determined from the solution within the domain $\left(\vec{V}_b = \vec{V}_d\right)$ Symmetry boundary condition $(\vec{n}.\nabla\vec{u} = 0)$ is imposed at X<0,Y=0 where, $\vec{n}$ is the unit normal vector. The scramjet walls are assumed adiabatic.

The impact of grid resolution on the wall surface pressure and determination of the lowest necessary resolution for accurate results is investigated through the generation of three grids with varying cell numbers. The details of the studied grids are shown in Table 1 and the freestream variables for the flow are M_∞=6.0, P_∞=488*Pa* and T_∞=51*K*. From Fig. 3(b), it can be observed that the grid is refined near the wall boundaries and near the isolator exit. This is achieved through the use of an adaptive grid resolution technique, which enhances the solution accuracy by refining the grid near the wall surfaces and near the flap deployment area.

Table 1. Different grid sizes used for grid independence test

Grid size	Number of cells
Coarse	68000
Medium	94000
Fine	117000

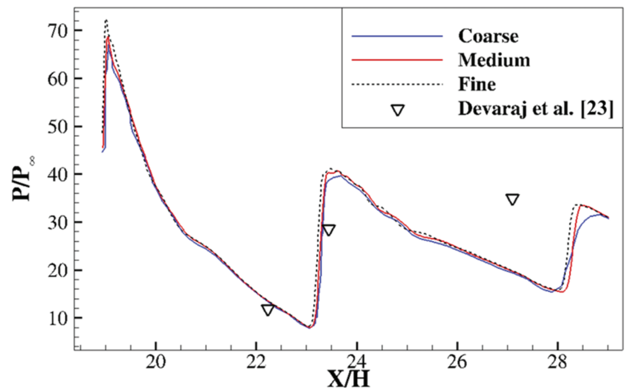

(a)

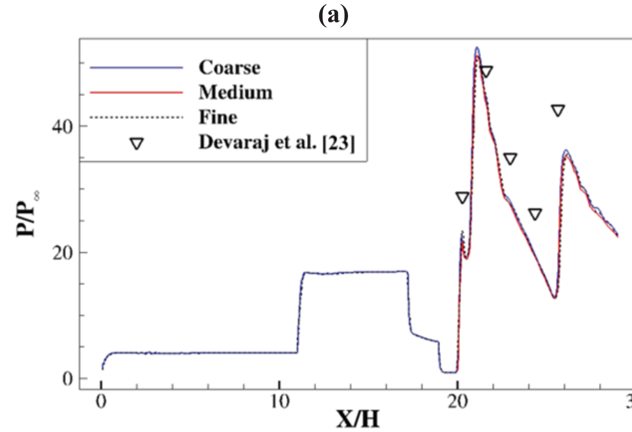

(b)

Figure 4. Comparison of normalized surface pressures obtained from fine, medium and coarse grids for (a) cowl and (b) ramp along with experimental results of Devaraj[23], *et al.*

In the present work, we employ geometry-based refinement to add resolution near the immersed boundary which is found to produce less oscillatory distribution of surface properties of interest. To reduce the discontinuity in cell sizes, it is ensured that at least 2 layers of similar size cell exist between different levels of refined cells.

The normalized surface pressures for the cowl and the ramp surfaces are displayed in Fig. 4 (a) and (b) respectively, indicating that the results are independent of any grid related uncertainties. Hence, the medium grid with a minimum cell length of 1.25×10^{-4} is used for the rest of the computations. Here, length in the x-direction is non-dimensionalized with respect to the height of the isolator. The surface pressures are also compared with that of the experimental data of Devaraj[23], *et al.* and reasonable agreement is observed between the numerical and experimental data. The observed discrepancies in the values can be attributed to the utilization of an inviscid solver, which neglects the influence of viscous effects.

3. RESULTS AND DISCUSSIONS

In this section, the started and unstarted flow conditions are described separately. The results are classified into started and unstarted mode, showing the two possible phenomena.

3.1 Intake Started state

Firstly, the flow field for the supersonic flow throughout the inlet is presented, under the freestream conditions, without the activation of the flap. The flap throttle (FT) percentage, presented here, is expressed as the flap's coverage of the exit isolator area to the total isolator height which serves as a non-dimensional parameter to represent the flap's location. The external and internal shock structures in the intake are shown in Fig. 5(a). Multiple shock reflections within the isolator are visible as expected, in a smooth and systematic manner. Flow undergoes compression through the ramp based oblique shocks and enters the intake with minimum spillage around the cowl. The corresponding Mach number contour is presented in Fig. 5(b). It is indicated by the Mach number contour that the flow reaching the end of the isolator is supersonic, with an average value of M_{exit}=2.5 at X/L=1.0. Thus, it can be remarked as a started inlet.

As the flap of the isolator exit is moved upwards to throttle the flow, the exit area is reduced. This is shown by using numerical schlieren images in Fig. 6 for different flap positions. The corresponding pressure contours, for the different FT states are plotted in Fig. 7. The case without the application of the flap is shown in Fig. 6(a). Due to the introduction of the flap, an oblique shock is generated at the isolator as shown in Fig. 6(b), from FT = 20 % onwards.

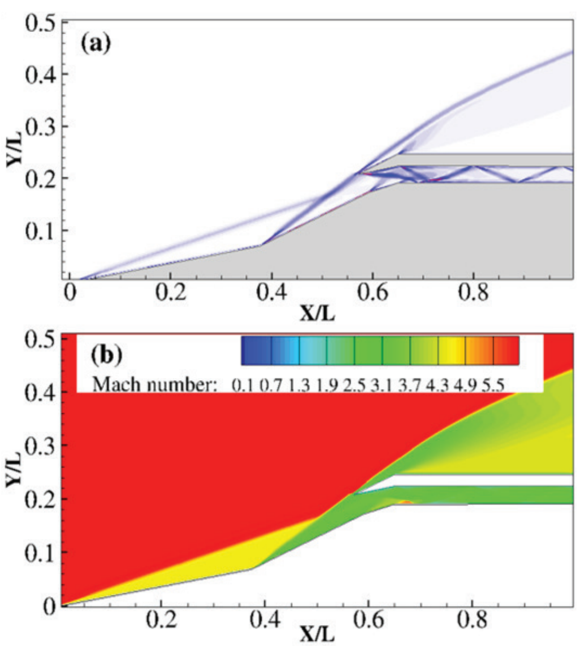

Figure 5. (a) Numerical density gradient schlieren and (b) Mach number contour, displaying the formation of the shocks for started state.

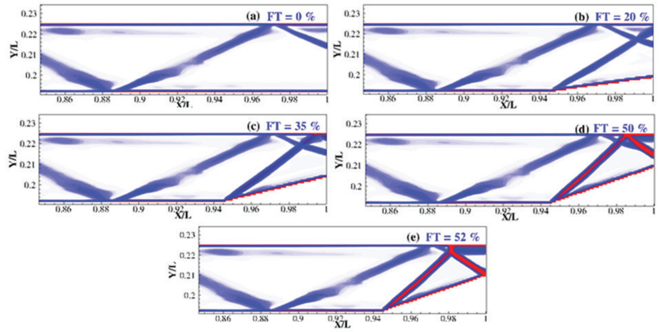

Figure 6. Numerical density gradient schlieren images of the isolator aft for different flap throttling (FT) states.

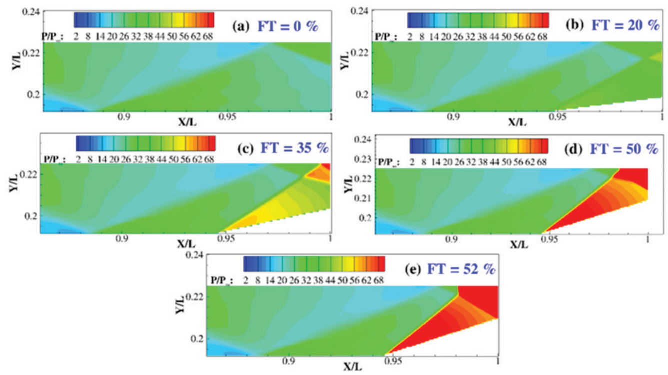

Figure 7. Normalized pressure contours of the isolator aft for different flap throttling (FT) states.

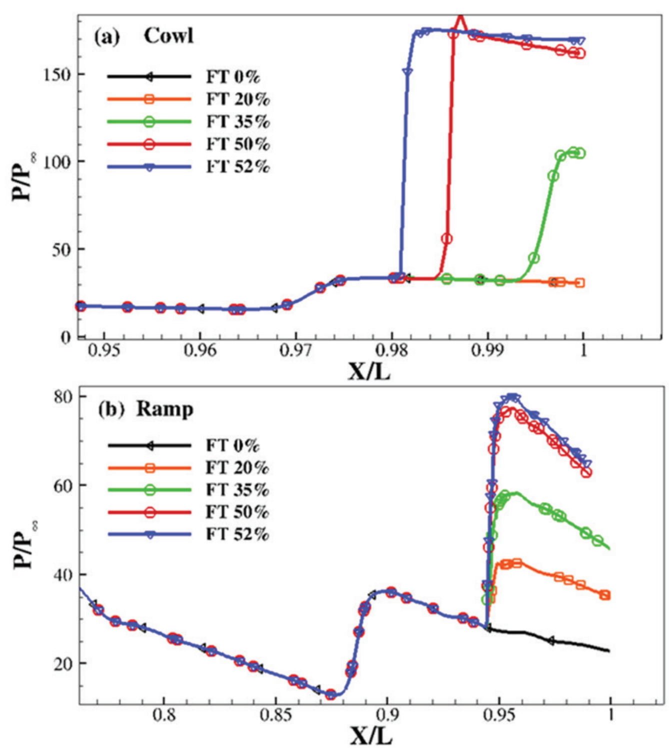

Figure 8. Normalized surface pressure on (a) the cowl side and (b) the ramp side for different flap throttling (FT) states.

An increment in the flow deflection angle (θ) is resulted in by the shifting of the flap in upward direction, leading to a corresponding increase in the angle of the shock wave angle (β) (Fig. 9). With further rise of the flap, at FT = 52 %, Mach

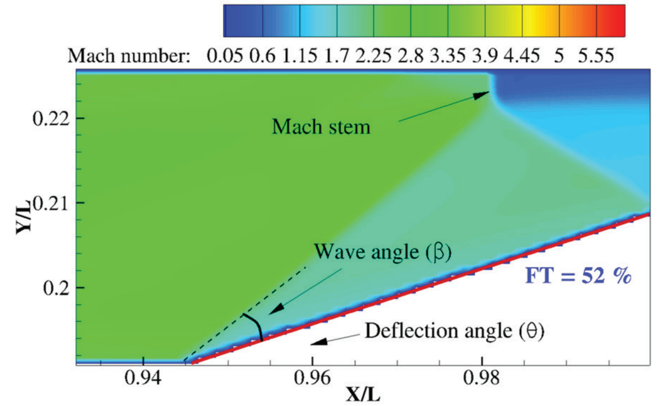

Figure 9. Mach number contour showing point of Mach reflection near the isolator ceiling for FT = 52 %.

reflection occurs near the ceiling of the isolator as is clearly visible from Fig. 9. A Mach reflection happens when a shock wave hits a surface with a limited angle and fails to redirect the flow to the desired extent. Specifically, the angle by which the flow is turned at the given Mach number is less than the angle of the surface (flap) it encounters.

The normalized surface pressures on the cowl and the ramp surfaces are presented in Fig. 8 (a) and (b), respectively. In both the plots, an increment in the surface pressures is observed with the increase in flat throttling (FT) states as expected with the raising of the flap. It is observed that with as the FT increases from 0 % to 52 %, the normalized static pressure increases from 25 to 160 on the cowl (Fig. 8.a) at and the same is observed to increase from 30 to 80 at X/L=0.95 on the ramp (Fig. 8(b)). Higher surface pressures are noted on the cowl side due to the impingement of the shock on the cowl surface corresponding to FT of 35 %, 50 % and 52 % (Fig. 7(c), (d), and (e)). Further, by increasing the flap deflection angle, the shock wave angle increases and the shock impingement location advances upstream. This is observed in the plots (Fig. 8) where the jump in surface pressures advances for higher FT values.

3.2 Intake Unstarted State

As flap is moved further upwards to obtain a throttling of FT = 53 %, a sudden spike in pressure is visible at the downstream of the Mach stem. This is evident from Fig. 10.a, where exit normalized pressure ratio reaches 340 times of the freestream values. This sudden pressure build-up suggests the presence of unstart shock waves near the flap. The onset of unstart is accompanied by a sudden flow reversal occurs at the isolator exit and the flow reverses towards the cowl.

Once the unstart shockwave structures form, it moves upstream because the strong adverse pressure gradient cannot support it and the flow is ultimately spilled about the cowl. This phenomenon is termed as inlet 'unstart' where the flow cannot pass through the isolator and hence, spills.

An instantaneous numerical density schlieren image of the unstart occurrence is presented in Fig. 10(b). The relative Mach number contour is provided in Fig. 10(c), that depicts that the flow is no more supersonic at the isolator exit which is not suitable for working of a scramjet combustor. A summarized table for the working modes with the corresponding flap position is presented in Table 2. Thus, by the use of IBM method, the flap was moved and was able to initiate unstart of the engine.

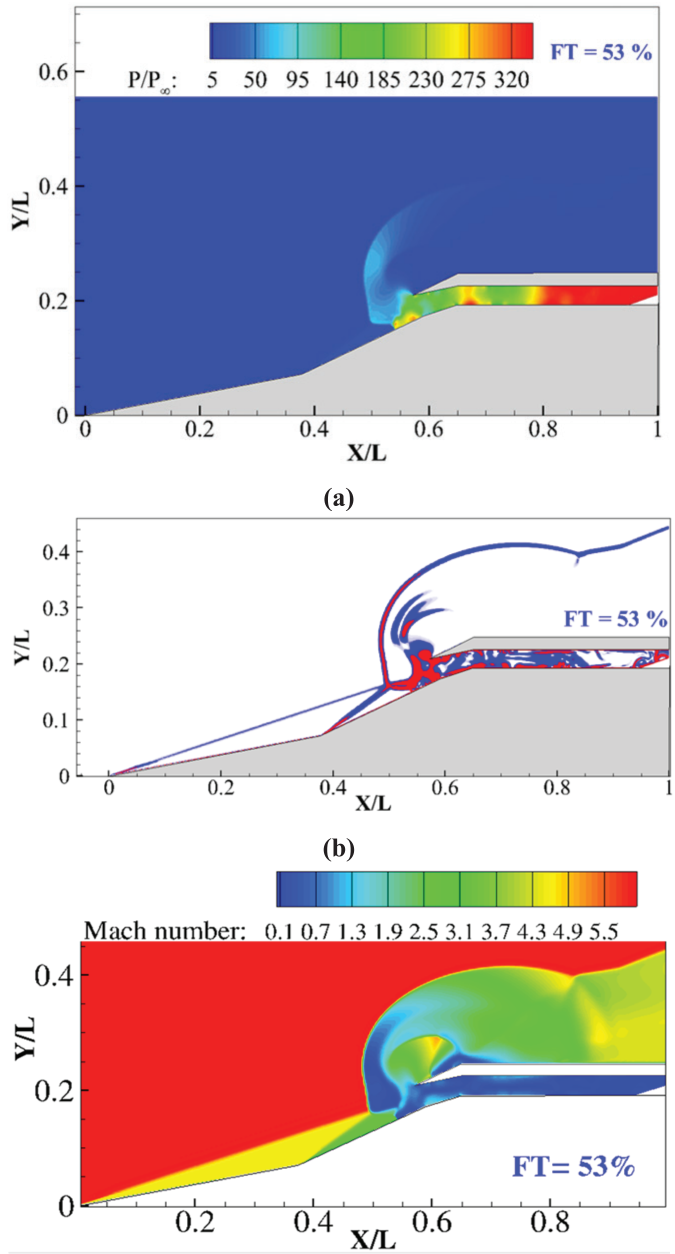

(c)

Figure 10. (a) Normalized pressure contour; (b) numerical density gradient schlieren; and (c) Mach number contour displaying the flow spillage around the cowl for unstarted inlet.

Table 2. Inlet mode of operation for different flap positions

Flap throttling percentage	Inlet operation mode
0	Started
20	Started
35	Started
50	Started
52	Started
53	Unstarted

4. CONCLUSIONS

Throttled flow is numerically studied in a scramjet inlet isolator by employing a movable flap placed at isolator exit. A two-dimensional Euler compressible CFD in-house Finite volume solver employing the AUSM scheme for resolving the convective fluxes, has been employed, to understand the deployment of flap in order to mimic high pressures generated in a scramjet combustor. Adaptive grid resolution method is utilized for the construction of the meshes and the body boundaries have been reconstructed using the Immersed Boundary Method (IBM). The in-house solver is successfully validated against a hypersonic testcase for flow over a hemispherical body and a satisfiable quantitative agreement is observed between the numerical and analytical data for the shock structure and the surface pressure coefficient.

Further, the validated solver is utilized to study the scramjet model for different flap locations. The scramjet model is run for flap less condition and it is observed to be in started condition with an exit Mach number of 2.5. By deploying the flap at different throttling positions, starting from 20 % and increasing till 52 %, the inlet is noted to be in started condition. Pressure plots clearly depicted the increase in isolator exit pressures at the cowl reaching up to 150 times of the freestream pressure with an advancement of the flap. A Mach stem is detected on the isolator ceiling when the throttling reaches 52 %. A further advance of the flap to throttling ratio of 53 % results in a complete flow reversal through the isolator causing into flow expulsion around the cowl.

REFERENCES

1. McClinton, C.R.; Rausch, V.L.; Shaw, R.J., Metha, U. & Naftel, C. Hyper-X: Foundation for future hypersonic launch vehicles. *Acta Astronaut.*, 2005, **57**(2-8), 614-622. doi: 10.1016/j.actaastro.2005.03.061
2. Baccarella, D.; Liu, Q.; McGann, B. & Lee, T. Isolator shock dynamics of mass injection-induced unstart in a circular model scramjet. *In* 23rd AIAA International Space Planes and Hypersonic Systems and Technologies Conference, 2020. doi: 10.2514/6.2020-2428
3. Reardon, J.P.; Schetz, J.A. & Lowe, K.T. Computational analysis of unstart in variable-geometry inlet. *J. Propuls. Power*, 2021, **37**(4), 564-576. doi: 10.2514/1.B38214
4. Hutchins, K.E.; Akella, M.R.; Clemens, N.T.; Donbar, J.M. & Gogineni, S. Experimental identification of transient dynamics for supersonic inlet unstart. *J. Propuls. Power*, 2014, **30**(6), 1605-1612. doi: 10.2514/1.B35230
5. Wagner, J.L.; Yuceil, K.B.; Valdivia, A.; Clemens, N.T. & Dolling, DS. Experimental investigation of unstart in an inlet/isolator model in Mach 5 flow. *AIAA J.*, 2009, **47**(6), 1528-1542. doi: 10.2514/1.40966
6. Noraiz, M. & Paolo, G. Understanding and modeling unstarting phenomena in a supersonic inlet cascade. *Phys. Fluids*, 2023, **35**(10), 106101. doi: 10.1063/5.0160706
7. Tan, H.J.; Li, L.G.; Wen, Y.F. & Zhang, Q.F. Experimental investigation of the unstart process of a generic hypersonic inlet. *AIAA J.*, 2011, **49**(2), 279-288. doi: 10.2514/1.J050200
8. Wang, K., Wang, J.Y., Huang, H.X., Xie, L.R., Liu, Y. & Tan, H.J. Effects of backpressure on unstart and restart characteristics of a supersonic inlet. *Aeronaut J.*, 2023, **127**(1316), 1774-1792. doi:10.1017/aer.2023.19
9. Do, H.; Im, S.K.; Mungal, M.G. & Cappelli, M.A. Visualizing supersonic inlet duct unstart using planar laser Rayleigh scattering. *Exp. Fluids*, 2011, **50**, 1651-1657. doi: 10.1007/s00348-010-1028-4
10. Xie, W. Z.; Ma, G.F.; Guo, R.W.; Chen, H.; Wen, Y.F. & Guo, S. Flow-based prediction for self-starting limit of two-dimensional hypersonic inlets. *J. Propuls. Power*, 2016, **32**(2), 463-471. doi: 10.2514/1.B35703
11. Dalle, D.J.; Fotia, M.L. & Driscoll, J.F. Reduced-order modeling of two-dimensional supersonic flows with applications to scramjet inlets. *J. Propuls. Power*, 2010, **26**(3), 545-555. doi: 10.2514/1.46521
12. Chang, J.; Yu, D.; Bao, W.; Fan, Y. & Shen, Y. Effects of boundary-layers bleeding on unstart/restart characteristics of hypersonic inlets. *Aeronaut. J.*, 2009, **113**(1143), 319-327. doi: 10.1017/S0001924000002992
13. Do, H.; Im, S.K.; Mungal, M.G. & Cappelli, M.A. The influence of boundary layers on supersonic inlet flow unstart induced by mass injection. *Exp. Fluids*, 2011, **51**, 679-691. doi: 10.1007/s00348-011-1077-3
14. Zhang, Q.F.; Tan, H.J.; Chen, H.; Yuan, Y.Q. & Zhang, Y.C. Unstart process of a rectangular hypersonic inlet at different Mach numbers. *AIAA J.*, 2016, **54**(12), 3681-3691. doi: 10.2514/1.J055005
15. Tan, H.J.; Sun, S. & Yin, Z.L. Oscillatory flows of rectangular hypersonic inlet unstart caused by downstream mass-flow choking. *J. Propuls. Power*, **25**(1), 2009, 138-147. doi: 10.2514/1.37914
16. Ghias, R.; Mittal, R. & Dong, H. A sharp interface immersed boundary method for compressible viscous flows. *J. Comput. Phys.*, 2007, 225(1), 528-553. doi: 10.1016/j.jcp.2006.12.007
17. Tran, P.H. & Plourde, F. Computing compressible internal flows by means of an Immersed Boundary Method. *Comput. Fluids*, 2014, **97**, 21-30. doi: 10.1016/j.compfluid.2014.03.009
18. Liou, M.S. & Steffen Jr, C.J. A new flux splitting scheme. *J. Comput. Phys.*, 1993, 107(1), 23-39. doi: 10.1006/jcph.1993.1122
19. Blazek, J. Computational fluid dynamics: principles and applications. Butterworth-Heinemann, 2015.
20. Ganesh, M.A. & John B. Concentrated energy addition

for active drag reduction in hypersonic flow regime. *Acta astronaut.*, 2018, **142**, 221-231.
doi:10.1016/j.actaastro.2017.11.003

21. Billig, F.S. Shock-wave shapes around spherical-and cylindrical-nosed bodies. J. Spacecr Rockets, 1967, **4**(6), 822-823.
doi:10.2514/3.28969
22. Lees, L. Hypersonic flow. *In* 5th International Aeronautical Conference, Los Angeles, 1955, 241–276.
23. Devaraj, M.K.K.; Jutur, P.; Rao, S.M.; Jagadeesh G. & Anavardham, G.T. Experimental investigation of unstart dynamics driven by subsonic spillage in a hypersonic scramjet intake at Mach 6. *Phys. Fluids*, 2020, **32**(2), 026103.
doi: 10.1063/1.5135096

CONTRIBUTORS

Ms. Amrita Pathak is a Research Scholar in the Department of Mechanical Engineering, IIT Guwahati. Her areas of interest are Computational fluid dynamics in hypersonic aerodynamics. Her contribution in this research is: Problem Conceptualization, Solver development, validation and preparation of manuscript.

Mr Jubajyoti Chutia is a Research Scholar in the Department of Mechanical Engineering, IIT Guwahati. His areas of interest are Computational fluid dynamics in hypersonic aerodynamics. His contribution in this research is: Problem conceptualization, solver development.

Prof. Vinayak Kulkarni is a Professor in the Department of Mechanical Engineering, IIT Guwahati. His areas of interest are Experimental aerodynamics, High enthalpy flows, Measurement science.
His contribution in this research is: Problem conceptualization, investigation and Supervision.